Preprint CRN 97-01
CRN, Strasbourg, 1997

The NEMO 3 simulation program: Current status

R. Arnold[1] **and V.I. Tretyak**[2]

Centre de Recherches Nucléaires, BP 28, 67037 Strasbourg Cedex 2, France

Abstract

In this note we present a description of the main features concerning the code developed to simulate and interpret almost all types of events likely to be produced in the NEMO 3 apparatus.

[1]email: arnold@crncl2.in2p3.fr

[2]permanent address: Institute for Nuclear Research of the Ukrainian National Academy of Sciences, 252650 Kiev, Ukraine; email: kinr@sovam.com

1 Introduction

The aim of the NEMO 3 [1] simulation program is to predict as precisely as possible the response of the detector to the occurrence of various physical processes. Simulated events are used to test the reconstruction (pattern recognition) and analysis (event selection) programs. They are also used to study the acceptance of the detector to backgrounds and rare processes.

In an early stage, during the design of the experiment, this program was used for the observation of what happens to various events inside the detector, to compute acceptances and so to reveal possible weaknesses of the setup. An important parameter in the search for rare events such as $\beta\beta$ decays is the contribution of background events faking real events. Therefore the ability to simulate all relevant background processes using a precise description of the various materials and geometry of the detector is mandatory.

This note describes in detail some parts of the code developed in the framework of GEANT [2] for the simulation of events in the NEMO 3 detector:

- the geometry of the experimental setup described by a set of geometrical volumes characterised by parameters relating to the material filling these volumes. Some of these volumes are considered as sensitive detectors giving a response when hit by particles;

- the generation of the initial kinematics of the events. This part of the program provides the possibility to generate all various double beta decays (0ν, 2ν, Majorons) for most of the nuclei candidates for that process. Also internal background events (events originating from the foil made of the material under study) as well as external background events (decaying nuclei located inside or outside of the detector or external fluxes of elementary particles) may be generated;

- the transport of particles through the various regions of the setup. Although this is the task of the code developed by the authors of GEANT, important features useful to understand the behaviour of the events are intercepted by the user part of the program during the stepping of the particles through the setup (interactions of the particles with wires, tracks hitting the source foil for example);

- the recording of tracks produced by particles hitting sensitive detectors and the description of the response of these detectors. This part involves the modeling of electronic signals (pulse shapes for example) leading to the digitisations after analog to digital or/and time to digital conversion;

- the visualization of the detectors. The possibility to observe the real particle trajectories together with the resulting digitisations is a helpful tool for the interpretation of the detector response. Creation and modification of tracks by picking up digitisations on the screen is very useful when testing pattern recognition programs and to rescue some of the pathological events.

2 The model of NEMO 3 used for the simulation

The description of the NEMO 3 device was done using the available drawings produced for the construction of the detector, created with the EUCLID industrial software [3], and the EUCLID–GEANT interface [4]. In this way it was possible to retrieve directly on the screen the dimensions, positions and rotations of the EUCLID objects, to create the corresponding GEANT volumes and to place them in correct positions using all possibilities of EUCLID to manipulate objects. Some complex EUCLID objects had to be divided into several parts because of the restricted number of shapes available in GEANT (EE scintillator blocks for example). In addition to the geometric information, the description of materials, tracking media and the hierarchy of volumes have been added. The EUCLID–GEANT interface gave also the possibility to check the overlap between objects and complete inclusion of daughter volumes into mother volumes.

As a result, the ASCII file containing the NEMO 3 model consists of 2615 lines of description and includes 485 basic objects, 33 divisions, 525 rotation matrices; 40 materials and 16 tracking media are described, some of them – for future use (foils with various double beta emitters). The full number of objects in the model is about 100000; of them, 1940 are scintillator blocks for energy measurements and 39820 wires for particle tracking. Fig. 1 shows the full NEMO 3 model and fig. 2 represents one of the 20 sectors. All the sectors are identical except for the source foils which can be placed in any desired position of the detector.

3 The event generator

The event generator, named GENBB, gives the initial kinematics of particles in an event: the number of particles emitted, their types (e^+, e^-, γ, α etc.), momentum components and time of emission.

3.1 Double beta processes

GENBB describes double beta processes ($2\beta^-$ and $2\beta^+$ decays, electron capture with emission of positron $\varepsilon\beta^+$ and double electron capture 2ε) for 16 nuclides, the most promising candidates from the full list of 69 [5]. 2β transitions to the ground state (g.s.) as well as to a few excited 0^+ and 2^+ levels of the daughter nucleus are allowed:

^{48}Ca$\rightarrow^{48}$Ti	$2\beta^-$	g.s., 2_1^+, 2_2^+
^{58}Ni$\rightarrow^{58}$Fe	2ε, $\varepsilon\beta^+$	g.s., 2_1^+, 2_2^+
^{76}Ge$\rightarrow^{76}$Se	$2\beta^-$	g.s., 2_1^+, 0_1^+, 2_2^+
^{74}Se$\rightarrow^{74}$Ge	2ε, $\varepsilon\beta^+$	g.s., 2_1^+, 2_2^+
^{82}Se$\rightarrow^{82}$Kr	$2\beta^-$	g.s., 2_1^+, 2_2^+
^{94}Zr$\rightarrow^{94}$Mo	$2\beta^-$	g.s., 2_1^+
^{96}Zr$\rightarrow^{96}$Mo	$2\beta^-$	g.s., 2_1^+, 0_1^+, 2_2^+, 2_3^+
^{92}Mo$\rightarrow^{92}$Zr	2ε, $\varepsilon\beta^+$	g.s., 2_1^+, 0_1^+
^{100}Mo$\rightarrow^{100}$Ru	$2\beta^-$	g.s., 2_1^+, 0_1^+, 2_2^+, 0_2^+
^{106}Cd$\rightarrow^{106}$Pd	2ε, $\varepsilon\beta^+$, $2\beta^+$	g.s., 2_1^+, 2_2^+, 0_1^+
^{114}Cd$\rightarrow^{114}$Sn	$2\beta^-$	g.s.

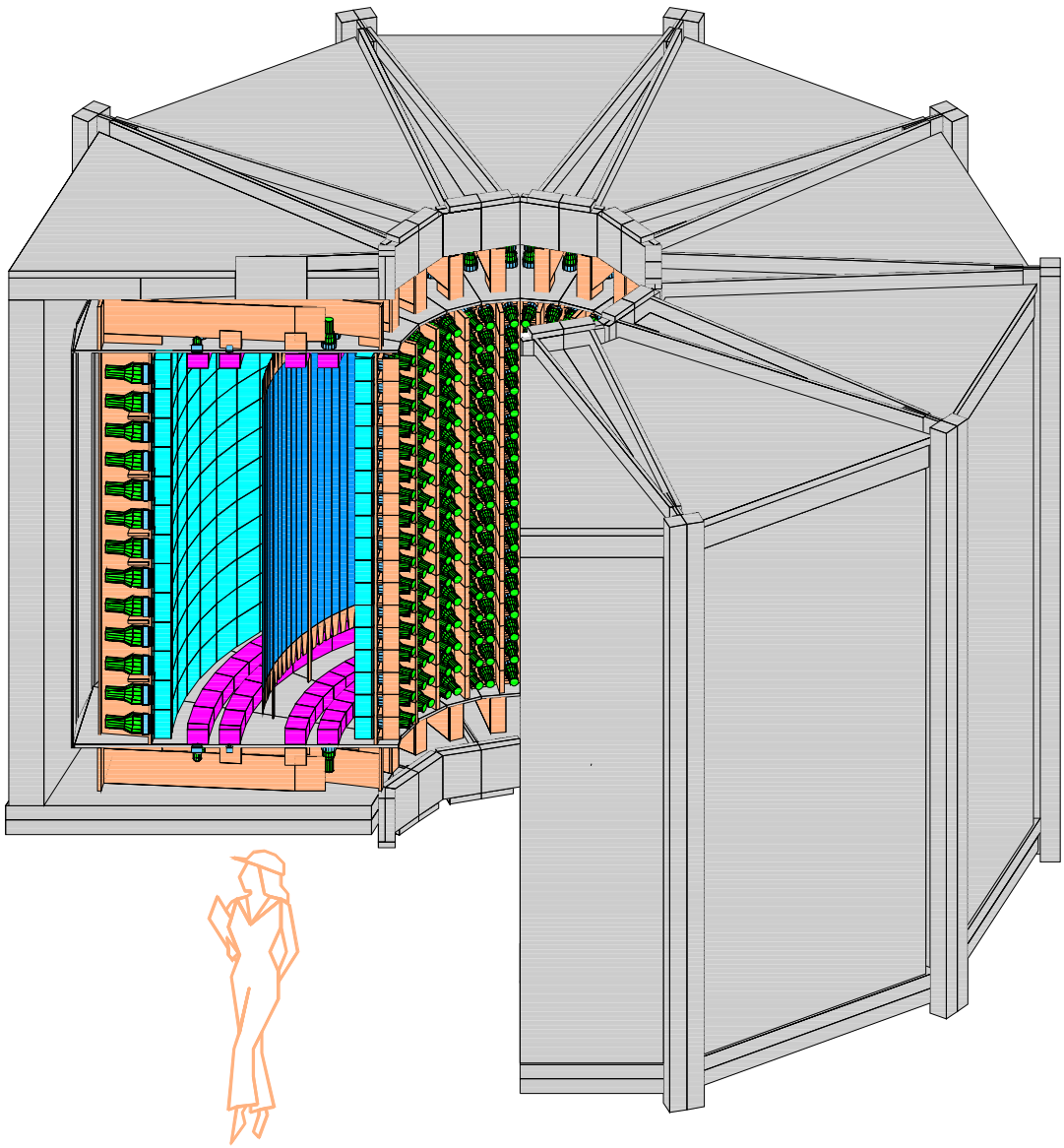

Figure 1: The model used in GEANT for the NEMO 3 installation. The detector and the coil are surrounded by an iron shield.

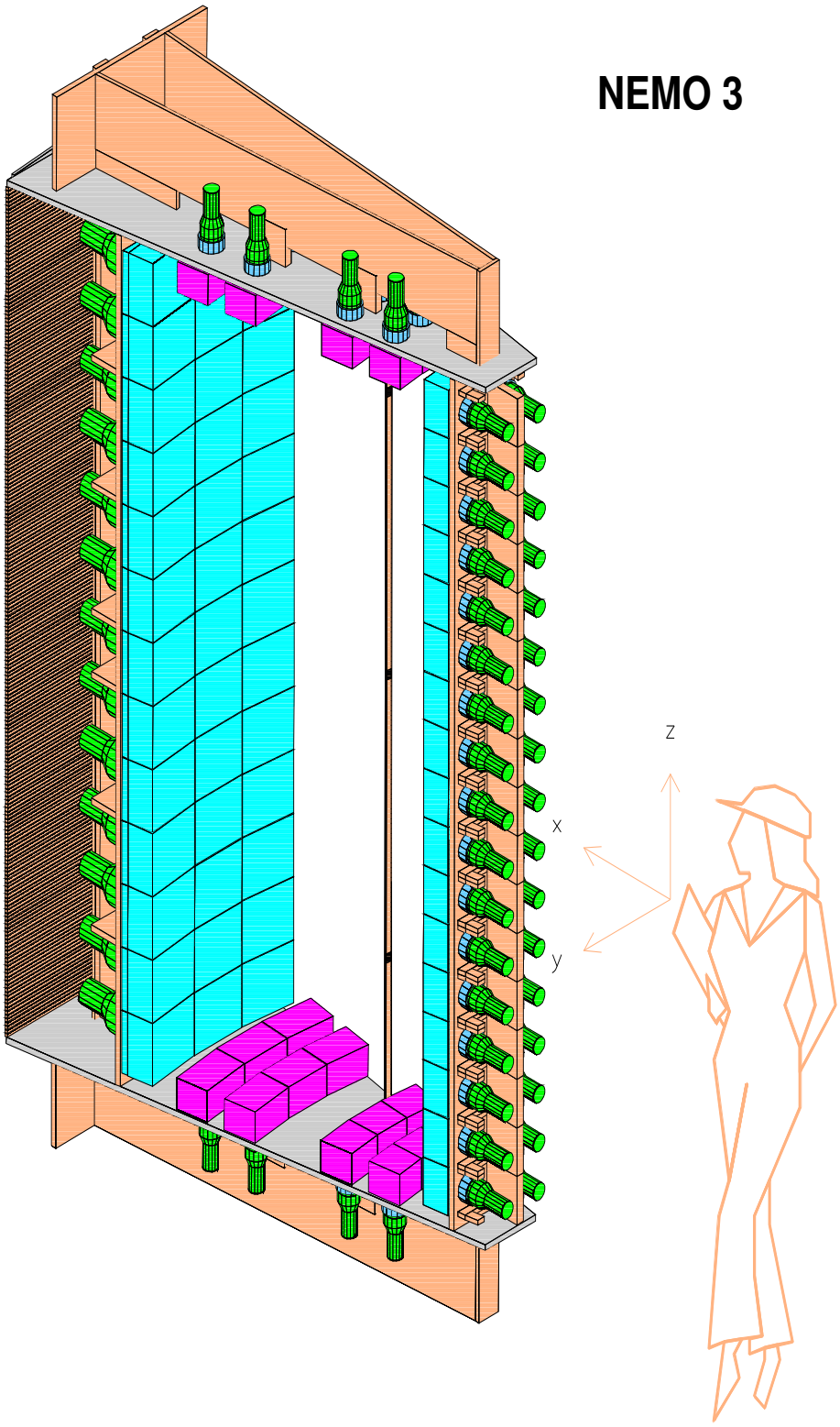

Figure 2: One sector of NEMO 3 as described in the geometry banks used by GEANT. The wires of the Geiger cells are not represented.

^{116}Cd$\rightarrow^{116}$Sn	$2\beta^-$	g.s., 2^+_1, 0^+_1, 0^+_2, 2^+_2, 2^+_3
^{130}Te$\rightarrow^{130}$Xe	$2\beta^-$	g.s., 2^+_1
^{136}Xe$\rightarrow^{136}$Ba	$2\beta^-$	g.s., 2^+_1, 2^+_2, 0^+_1
^{148}Nd$\rightarrow^{148}$Sm	$2\beta^-$	g.s., 2^+_1, 2^+_2
^{150}Nd$\rightarrow^{150}$Sm	$2\beta^-$	g.s., 2^+_1, 0^+_1, 2^+_2, 2^+_3, 0^+_2

Transitions to all levels of daughter nuclei, for which experimental results are known [5], are available in GENBB.

If 2β decay occurs to an excited level of a nucleus, the deexcitation process with emission of γ quanta, conversion electrons and e^+e^- pairs follows (see section 3.2 for the description of nuclear deexcitation process).

For each transition to the ground or an excited level, various modes (with emission of two neutrinos or Majoron, neutrinoless decays due to nonzero neutrino mass or right-handed admixture in the weak interaction etc.) and mechanisms (two-nucleon 2n and Δ-isobar N*) of double beta decay are possible. Below we give the theoretical formulae for the energy and angular distributions used in GENBB to sample the energies and angles of emitted electrons or positrons. The Primakoff-Rosen (PR) approximation for the Fermi function, which takes into account the influence of the electric field of the nucleus on the emitted particles, is not used anymore in GENBB (it was used in earlier versions [6]) to describe accurately the energy spectra not only of electrons in $2\beta^-$ decay but also positrons in $2\beta^+$ and $\varepsilon\beta^+$ decays. See [7], [8] and [9] for comparison of exact distributions with those calculated in the PR approximation.

The sampling of energies and angles of e^- or e^+ is based on 3-dimensional distributions $\rho_{12\theta}(t_1, t_2, cos\theta)$, where t_i is the kinetic energy of the i-th e^- or e^+ (all energies in this section are in units of the electron mass m_0c^2) and θ is the angle between the particle directions, from which 2-dimensional energy distributions $\rho_{12}(t_1, t_2)$ and 1-dimensional distributions $\rho_1(t_1)$ are calculated:

$$\rho_{12}(t_1, t_2) = \int_0^{\pi} \rho_{12\theta}(t_1, t_2, cos\theta)\, d(cos\theta), \tag{1}$$

$$\rho_1(t_1) = \int_0^{t_0 - t_1} \rho_{12}(t_1, t_2)\, dt_2. \tag{2}$$

In these expressions t_0 is the energy available in the 2β process: for $2\beta^-$ decay t_0=$Q_{\beta\beta} - E_{level}$, for $2\beta^+$ decay t_0=$Q_{\beta\beta} - 4 - E_{level}$, for $\varepsilon\beta^+$ decay t_0=$Q_{\beta\beta} - 2 - E_B - E_{level}$ and for 2ε decay $t_0 = Q_{\beta\beta} - E_{B_1} - E_{B_2} - E_{level}$, where $Q_{\beta\beta}$ is the energy release (mass difference between parent and daughter atoms [10]), E_{level} the energy of excited level of daughter nucleus, and E_{B_j} the binding energies of electrons on the atomic shell.

The energy of the first e^- or e^+ is sampled in accordance with (2), after the energy of the second particle is sampled from (1) with fixed t_1 and finally the angle θ is sampled from $\rho_{12\theta}(t_1, t_2, cos\theta)$ with fixed t_1 and t_2 (supposing isotropic emission for the first particle) [11]. The GENBB distributions $\rho_{12\theta}(t_1, t_2, cos\theta)$ are based on works [12], [13], [14], [15] and [16] (the PR approximation in [12] was removed). Without the PR approximation, the integrals (2) for some modes cannot be derived analytically, so they are calculated numerically in GENBB. Analytical expressions for 2β distributions in the PR approximation can be found in [5].

The momentum of the i-th electron, p_i, which appears in the formulae below is given by $p_i = \sqrt{t_i(t_i+2)}$ (in units of m_0c) and its velocity, β_i, by $\beta_i = p_i/e_i$ (in units of c) where $e_i = t_i + 1$. The Fermi function is defined as

$$F(t,Z) = const \cdot p^{2s-2} exp(\pi\eta) \mid \Gamma(s+i\eta) \mid^2, \tag{3}$$

where $s = \sqrt{1-(\alpha Z)^2}$, $\eta = \alpha Ze/p$, $\alpha = 1/137.036$, Z is the atomic number of the daughter nucleus ($Z > 0$ for β^- and $Z < 0$ for β^+ decay) and Γ the gamma function. In the PR approximation $F(t,Z) \sim e/p$, which is adequate only for $Z > 0$ (β^- and $2\beta^-$ decays).

1. $0\nu 2\beta^{\pm}$ decay with neutrino mass, $0^+ - 0^+$ transition, $2n$-mechanism

$$\rho_{12\theta}(t_1,t_2,cos\theta) = e_1p_1F(t_1,Z)e_2p_2F(t_2,Z)\delta(t_0-t_1-t_2)(1-\beta_1\beta_2cos\theta), \tag{4}$$

$$\rho_{12}(t_1,t_2) = e_1p_1F(t_1,Z)e_2p_2F(t_2,Z)\delta(t_0-t_1-t_2). \tag{5}$$

2. $0\nu 2\beta^{\pm}$ decay with right-handed currents, $0^+ - 0^+$ transition, $2n$-mechanism

$$\rho_{12\theta}(t_1,t_2,cos\theta) = e_1p_1F(t_1,Z)e_2p_2F(t_2,Z)(t_1-t_2)^2\delta(t_0-t_1-t_2)(1+\beta_1\beta_2cos\theta), \tag{6}$$

$$\rho_{12}(t_1,t_2) = e_1p_1F(t_1,Z)e_2p_2F(t_2,Z)(t_1-t_2)^2\delta(t_0-t_1-t_2). \tag{7}$$

3. $0\nu 2\beta^{\pm}$ decay with right-handed currents, $0^+ - 0^+$ and $0^+ - 2^+$ transitions, N^*-mechanism

$$\rho_{12\theta}(t_1,t_2,cos\theta) = p_1F(t_1,Z)p_2F(t_2,Z)[2p_1^2p_2^2cos^2\theta - p_1p_2cos\theta\{(e_1+e_2)^2 + \tag{8}$$

$$+4(e_1e_2+1)\} + 3(e_1e_2+1)(p_1^2+p_2^2)]\delta(t_0-t_1-t_2),$$

$$\rho_{12}(t_1,t_2) = p_1F(t_1,Z)p_2F(t_2,Z)[2p_1^2p_2^2 + 9(e_1e_2+1)(p_1^2+p_2^2)]\delta(t_0-t_1-t_2). \tag{9}$$

The formulae for $0^+ - 0^+$ and $0^+ - 2^+$ transitions in this mode of decay are the same but the value of t_0 differs by E_{level}.

4. $2\nu 2\beta^{\pm}$ decay, $0^+ - 0^+$ transition, $2n$-mechanism

$$\rho_{12\theta}(t_1,t_2,cos\theta) = e_1p_1F(t_1,Z)e_2p_2F(t_2,Z)(t_0-t_1-t_2)^5(1-\beta_1\beta_2cos\theta), \tag{10}$$

$$\rho_{12}(t_1,t_2) = e_1p_1F(t_1,Z)e_2p_2F(t_2,Z)(t_0-t_1-t_2)^5. \tag{11}$$

5. $0\nu 2\beta^{\pm}$ decay with emission of Majoron, $0^+ - 0^+$ transition, $2n$-mechanism

For $0\nu 2\beta$ decay with emission of Majoron [17]

$$\rho_{12\theta}(t_1,t_2,cos\theta) = e_1p_1F(t_1,Z)e_2p_2F(t_2,Z)(t_0-t_1-t_2)(1-\beta_1\beta_2cos\theta), \tag{12}$$

$$\rho_{12}(t_1, t_2) = e_1 p_1 F(t_1, Z) e_2 p_2 F(t_2, Z)(t_0 - t_1 - t_2). \quad (13)$$

6. $0\nu 2\beta^{\pm}$ decay with double Majoron emission, $0^+ - 0^+$ transition, $2n$-mechanism; decay with charged $L = -2$ Majoron and massive vector Majoron

For both decay with double Majoron emission [13] and decay with emission of Majoron with lepton number -2 [14]

$$\rho_{12\theta}(t_1, t_2, cos\theta) = e_1 p_1 F(t_1, Z) e_2 p_2 F(t_2, Z)(t_0 - t_1 - t_2)^3 (1 - \beta_1 \beta_2 cos\theta), \quad (14)$$

$$\rho_{12}(t_1, t_2) = e_1 p_1 F(t_1, Z) e_2 p_2 F(t_2, Z)(t_0 - t_1 - t_2)^3. \quad (15)$$

For the decay with emission of a vector Majoron with mass m [15]

$$\rho_{12\theta}(t_1, t_2, cos\theta) = e_1 p_1 F(t_1, Z) e_2 p_2 F(t_2, Z)[(t_0 - t_1 - t_2)^2 - m^2]^{3/2} (1 - \beta_1 \beta_2 cos\theta). \quad (16)$$

In the $m = 0$ case this distribution (and all subsequent ones) reduces to the distribution for double Majoron emission.

7. $0\nu 2\beta^{\pm}$ decay with right-handed currents, $0^+ - 2^+$ transition, $2n$-mechanism

$$\rho_{12\theta}(t_1, t_2, cos\theta) = p_1 F(t_1, Z) p_2 F(t_2, Z)[3 p_1^2 p_2^2 cos^2\theta - p_1 p_2 cos\theta (10(e_1 e_2 + 1) + \quad (17)$$

$$+ p_1^2 + p_2^2) + 5(e_1 e_2 + 1)(p_1^2 + p_2^2) - p_1^2 p_2^2] \delta(t_0 - t_1 - t_2),$$

$$\rho_{12}(t_1, t_2) = p_1 F(t_1, Z) p_2 F(t_2, Z)(e_1 e_2 + 1)(p_1^2 + p_2^2)] \delta(t_0 - t_1 - t_2). \quad (18)$$

8. $2\nu 2\beta^{\pm}$ decay, $0^+ - 2^+$ transition, $2n$- and N^*-mechanism

$$\rho_{12\theta}(t_1, t_2, cos\theta) = e_1 p_1 F(t_1, Z) e_2 p_2 F(t_2, Z)(t_1 - t_2)^2 (t_0 - t_1 - t_2)^7 (1 + \frac{1}{3} \beta_1 \beta_2 cos\theta), \quad (19)$$

$$\rho_{12}(t_1, t_2) = e_1 p_1 F(t_1, Z) e_2 p_2 F(t_2, Z)(t_1 - t_2)^2 (t_0 - t_1 - t_2)^7. \quad (20)$$

The formulae for the N^*-mechanism in this mode of decay are the same as for the $2n$-mechanism.

9. $0\nu \mathrm{K}\beta^+$ decay, $0^+ - 0^+$ and $0^+ - 2^+$ transitions

Only K-shell electron capture is considered in GENBB. In $0\nu \mathrm{K}\beta^+$ decay a monoenergetical positron is emitted (with energy $t_0 = Q_{\beta\beta} - 2 - E_K - E_{level}$). The hole in the atomic K shell, created in the K-electron capture, results in emission of an X ray with energy E_K. Both particles are emitted isotropically without any angular correlation.

10. $2\nu\mathbf{K}\beta^+$ decay, $0^+ - 0^+$ and $0^+ - 2^+$ transitions

This process is similar to usual β^+ decay but two neutrinos are emitted instead of one. The distribution for a continuous positron energy spectrum is given [16] by

$$\rho_1(t_1) = e_1 p_1 F(t_1, Z)(t_0 - t_1)^5. \tag{21}$$

An X ray with energy E_K is also emitted (as in the previous section).

11. 0ν2K decay, $0^+ - 0^+$ and $0^+ - 2^+$ transitions

Because no neutrinos are emitted, it is supposed that all energy release is taken by one γ quantum with energy $t_0 = Q_{\beta\beta} - 2E_K - E_{level}$. Two X rays with energy E_K are also emitted; no angular correlation is supposed between the particles.

12. 2ν2K decay, $0^+ - 0^+$ and $0^+ - 2^+$ transitions

Two X rays with energy E_K are emitted without angular correlation. In the case of a transition to an excited level of the daughter nucleus, additional particles (γ, conversional e^- and e^+e^- pairs) will be emitted.

3.2 Decay of natural radioactive nuclides

The presence of admixtures of natural radioactive nuclides in the foil under investigation is very dangerous: in their decay, events could be produced which imitate double beta decay. In the last process two e^- (or e^+) are emitted at the same place and time with specific energy and angular distributions (see section 3.1). In decays of nuclides from the natural radioactive chains two e^- (e^+) can also be emitted (practically) simultaneously and (practically) in the same place: in general the first e^- (e^+) is emitted in a β decay (most of these nuclides are β decayers); the second e^- can be created after Möller (Bhabba) scattering of the first e^- (e^+), or, if an excited level of the daughter nucleus resulted from the β decay, in nuclear deexcitation when a conversion electron or e^-e^+ pair is emitted instead of a γ quantum. Compton scattering or photoeffect of a deexcitation γ quantum in the neighbourhood gives also a second electron. Such events will result, if not in a full imitation of 2β decays, at least in a two electron background. Therefore simulation of the decay of dangerous nuclides is necessary to know the efficiencies and response functions of the NEMO 3 detector for the corresponding 2e events. Description of nuclide decays should be very detailed and precise [18] remembering that the NEMO 3 experiment is aimed at searching for extremely rare processes (4.2 $2\beta0\nu$ decays occur in 10 kg of ^{100}Mo per year if $T^{0\nu}_{1/2} = 10^{25}$ y).

The event generator also provides the possibility to generate events from the decay of some artificial isotopes which are used as calibration sources – to simulate the calibration of the detector and check with good statistics the simulated efficiencies and spectra shapes.

The current list of background and calibration isotopes includes 26 nuclei:

^{228}Ac	^{152}Eu	^{214}Pb
^{207}Bi+^{207m}Pb	^{154}Eu	^{106}Rh

^{208}Bi	^{146}Gd	^{90}Sr
^{210}Bi	^{182}Hf	^{182}Ta
^{212}Bi+^{212}Po	^{40}K	^{207}Tl
^{214}Bi+^{214}Po	^{22}Na	^{208}Tl
^{60}Co	^{234m}Pa	^{88}Y
^{137}Cs+^{137m}Ba	^{211}Pb	^{90}Y
^{147}Eu	^{212}Pb	

All probabilities for α and β decay modes, values of energy release, energies of excited nuclear levels and probabilities of transitions to lower levels are taken from [19]. Energies are rounded off to 1 keV and probabilities to 0.001% (decays and transitions with probabilities less than 0.001% are not taken into account). To describe the deexcitation process in the daughter nucleus, full nuclear schemes as described in [19] were used, without any approximations or simplifications (for ^{152}Eu and ^{154}Eu, models were constructed in accordance with the new edition of the "Table of Isotopes" [20] and with the corresponding issues of Nuclear Data Sheets). Such an approach leads sometimes to quite complex descriptions:

- for decay of ^{154}Eu, 31 levels of ^{154}Gd (^{154}Eu β^- decay), 2 levels of ^{154}Sm (^{154}Eu EC decay), and 164 different γ quanta are taken into account in the model;

- for decay of ^{214}Bi, 48 levels of ^{214}Po (^{214}Bi β^- decay), 3 levels of ^{210}Tl (^{214}Bi α decay) and 105 different γ quanta are included;

- for β^- decay of ^{228}Ac, the model contains 44 excited levels of ^{228}Th and 166 different γ quanta.

Some simplifications were made only in a few cases: for ^{234m}Pa (99.7% of the possible decay paths are described), for ^{214}Po (99.989%) and for ^{106}Rh (99.32%).

For each transition from an excited nuclear level to one of the lower levels, all three concurrent processes are taken into account in the models: (1) to emit a γ quantum; (2) to emit a conversion electron instead of a γ; (3) to emit an electron-positron pair (in this case the energy of the transition must be greater than 1.022 MeV). Such an approach allows automatically to consider the emission not only of one but of two or more conversion electrons and/or e^+e^- pairs, which is especially important from the point of view of 2β decay imitation.

Experimental data of [19] and [20] were used for coefficients of conversion of γ quanta to e^+e^- pairs; if such data were unavailable, graphs from [21] were used as a source of theoretical values. Emitted in internal pair e^+ and e^- are supposed to have equal energies and the same direction [22].

For values of coefficient of conversion of γ quanta to conversion electrons, the experimental data [19], [20] were used when available; if not, the values were determined from the theoretical curves in [23].

Only conversion from the K atomic shell was assumed in all cases when the transition energy was sufficient; if not, L (or even M) conversion was assumed. As a result of conversion, an electron with energy $E_{e^-} = E_\gamma - E_B$ and an X ray with energy E_B are emitted; Auger electrons are not considered (here E_γ is the energy of the corresponding γ quantum, and E_B the binding energy of an electron on the shell).

For ^{207}Bi+^{207m}Pb decay, a more sophisticated model was created taking into account the conversion from K, L and M atomic shells, emission of K, L and M X rays and K and

L Auger electrons.

Angular correlations between γ quanta in a cascade of nuclear transitions are not considered; all γ, conversional e^- and e^+e^- pairs are independent and emitted isotropically.

Non-zero half-life of excited levels leading to a delay in particles emission is taken into account.

All β decays to the ground and excited levels of the daughter nucleus are considered as allowed, and only the Fermi correction factor to the shape of the energy spectrum of β particles is taken into account: $\rho(t) = epF(t,Z)(t_0 - t)^2$, where e, p, F, t, Z are defined as in section 3.1 (now t_0 is equal to $Q_\beta - E_{level}$ for β^- and $Q_\beta - E_{level} - 2$ for β^+ decay).

3.3 Special events

In addition to 2β decays and decays of radioactive nuclei, some special events can also be produced.

Compton scattering of external γ quanta or Möller scattering of external e^- are simulated by GEANT itself but their occurrence in some cases (for a thin foil for example) is very low and the simulation of a prohibitive number of events must be done to obtain some spectra with sufficient statistics. The event generator provides the possibility of generating the kinematics of such events (for energy and angles of the initial γ or e^- in some given range) speeding up in this way the computations. In this case the absolute efficiency must be calculated by the user himself.

Artificial events with emission of up to 10 β particles, e^+e^- pairs or any kind of particle [2], including γ, e^-, e^+, μ^-, μ^+, α etc., can be produced. The ranges for their energies and directions are chosen by the user.

4 The tracking of particles

In GEANT tracking of a particle through a geometry of objects consists in calculating a set of points in a 7-dimensional space (x, y, z, t, p_x, p_y, p_z) which is called the trajectory of the particle. This is achieved by integrating the equations of motion over successive steps from one trajectory point to the next and applying corrections to account for the presence of matter. The simulation of particles traversing the setup has to take into account the interactions of those particles with the material of the detector. GEANT is able to simulate the dominant processes which can occur in the energy range from 10 keV to 10 TeV for electromagnetic interactions which are relevant in our case.

In our application it is supposed that a particle whose energy falls below the 10 keV limit is stopping. The selected processes which accompany the propagation of a particle through the material of the detector are:

Processes involving photons:
- e^+e^- pair conversion,
- Compton scattering,
- Photoelectric effect,
- Rayleigh scattering;

Processes involving e^-, e^+:

Multiple scattering,
Ionization and δ-rays production,
Bremsstrahlung,
Annihilation of positron.

Note that photo fission of heavy elements (no material with A>230 is present in our detector), generation of Čerenkov and synchrotron radiation are neglected but could be included without difficulty.

In addition to the physical effects the constraints of a geometrical nature lead to a set of tolerances influencing the tracking step size. These quantities can be calculated by the program itself but in order to avoid unacceptable losses of accuracy some of them have been fixed to the values listed in the appendix A.

At each step during the tracking of a particle the following actions are taken:

1. The secondary particles produced are stored for further tracking.

2. For electrons hitting a scintillator block some information is recorded:

- the coordinates of the point where the particle enters the block or where it is created inside the volume (by Compton scattering for example);
- the time of flight and the kinetic energy of the particle at the entry into the volume or the time of its creation (time 0 corresponds to the moment when the primary decay occurred);
- the energy loss of the particle inside the scintillator block.

3. For charged particles entering or created in a Geiger cell an average number of ionization electrons produced is calculated according to the energy lost in the cell. The actual number of electrons is taken from a Poisson distribution and their position is distributed randomly along the path of the particle. When the particle leaves the Geiger cell (or stops in it) the following information is stored:

- the coordinates of the ionization electron produced closest to the anode wire and its distance to that wire;
- the time when this electron was produced;
- the kinetic energy of the particle at its entry into the cell or at its creation point (for a Compton e^- or a δ ray for example);
- the total energy lost by the particle inside the cell.

4. The information listed above is used in a latter stage for the simulation of the detector digitisations. In order to go into the details on how the detector behaves, it is interesting to catch some additional information not (or at least not easily) accessible in the real experiment (interactions of the particles with the foil or with wires for example) such as:

- the coordinates of the point where the particle is starting or entering in the foil;
- the coordinates of the point where the particle is leaving the foil or stopping;
- the energy lost inside the foil;
- the momentum of a particle when it hits a wire;
- the momentum of that particle when it quits the wire or stops;
- the kinetic energy of the particle hitting a wire;
- the energy lost by the particle inside the wire.

These quantities were helpful to optimize the thickness of the foil and to study the effects resulting from the diameter and material of the wires [24].

5. Finally the coordinates of the space points generated during the tracking are stored. This information can be used latter for debugging purposes and for graphical representation of the particle trajectories.

5 The detector response

The simulation of the detector response requires digitisations for each detector element to be defined. These digitisations are computed after complete tracking of each event. This is done by using the hits recorded during tracking time to keep trace of the interaction between particles and detectors (see appendix B for the description of the content of the hit banks). The NEMO detector generates digitisations originating from the scintillators hit and digitisations induced by the Geiger cells hit.

1. Digitisations originating from the scintillators. These are:

- a detector identifier giving the address of the scintillator block hit (16 bits);
- a 12 bit word containing the value given by the ADC of the corresponding electronic channel;
- a 12 bit word containing the value given by the TDC of the corresponding electronic channel;
- a flag indicating if the signal was above the higher threshold level of the discriminator (the discriminators of the NEMO 3 have two levels of discrimination: the high level is used for triggering purposes and the low level allows the information from scintillators fired by X rays to be recorded if the event is accepted by the trigger).

2. Digitisations originating from the Geiger cells. These are:

- a detector identifier giving the address of the Geiger cell hit (16 bits);
- a 12 bit word containing the value given by the fast TDC of the corresponding anode wire;
- a 12 bit word containing the value given by the slow TDC of the corresponding anode wire. This information is only registered in the presence of a hit delayed by more than 4 microseconds with respect to the reference time (the reference signal (trigger) is supposed to be available about $\leq$ 50 ns after the occurrence of a signal from the first scintillator passing the high level discrimination);
- a 12 bit word containing the value from the TDC of the electronic channel of the cathode at the bottom of the (vertical) Geiger cell;
- a 12 bit word containing the value from the TDC of the electronic channel of the cathode at the top of the Geiger cell.

Both types of digitisations are coded in two 32 bit words as described in appendix B.

5.1 Scintillator digitisations

1. Energy information.

The hit information bank recorded during tracking time contains the energy deposited by a particle entering the scintillator blocks. Some blocks, of complicated shape (not available as a GEANT volume), are described by the union of two different sensitive volumes. For each block, the sum of the energy deposited by all particles is performed (for blocks described by two volumes the energy sum deposited in them is calculated). The energy resolution is calculated from the relation: $FWHM(E)/E = K/\sqrt{E}$ with the energy E expressed in MeV (K is the resolution at 1 MeV) and the energy sum distorted according to a gaussian resolution function. The resulting quantity is converted into a ADC channel number (2 keV/channel). The values of K depend on the size of the block and on the phototube used to collect the light; they vary from 0.120 for the outer wall blocks to 0.145 for the inner wall blocks according to measurements done in the laboratory.

2. Time information.

In contrast to double beta decays, where all particles are emitted isochronously (only for decays to an excited level of the daughter nucleus some particles are emitted after a short delay) and are thus visible in a single event, some nuclei decaying in cascade can produce particles during a large interval of time. Such processes are treated as follows. The first msec of the process is considered as an event in its own. After this first msec, particles produced during a fixed interval of time (corresponding to the dead time of the detector) are ignored. After that dead time the next particle produced restarts a new event lasting again a maximum of one msec. This algorithm is repeated until complete deexcitation of the last nucleus of the decay chain occurs. Thus an decay may lead to several separate detected events.

In the experiment, scintillator timing information is used to reject external events. It is therefore important for the simulation to reproduce rather accurately all instrumental effects affecting the timing and occurring between the moment when a particle hits the scintillator and the time when the signal is actually recorded.

2.1. Transit time fluctuations.

The following formula is used to describe the variance of the transit time fluctuations inside the phototubes:

$$\sigma^2 = (\sigma_t^2 + \sigma_{tt}^2)(1 + \sigma_{pmt}^2)/n_{phe}(E), \tag{22}$$

where σ_t^2 is the variance of the decay time ($\sigma_t^2 = \tau^2$ is used where τ is the decay time constant of the scintillator), σ_{tt}^2 is the variance of the transit time for one photoelectron, σ_{pmt}^2 is the relative variance of the PMT gain (calculated from the collection efficiency and the gain of the phototube), $n_{phe}(E)$ is the number of primary photoelectrons ($n_{phe}(E)$ is approximated by $(2.36/K)^2 \cdot E$ from the relation above giving the resolution).

The fig. 3a illustrates the variation and the fluctuation of the transit time as a function of the energy deposited in the scintillator blocks.

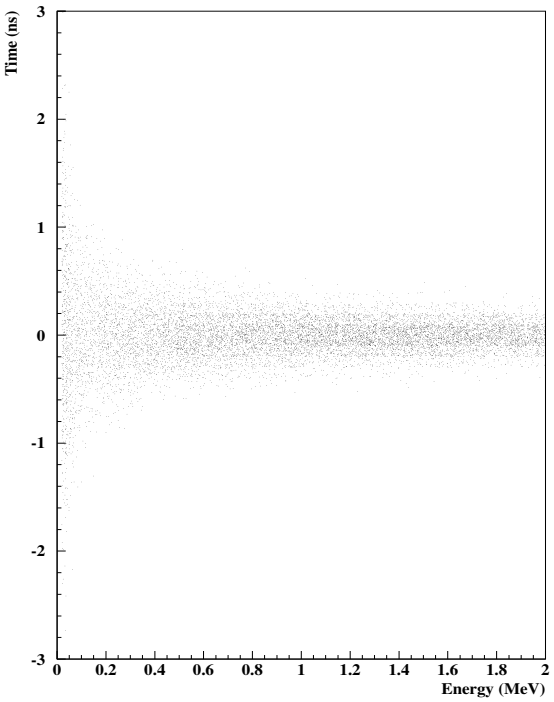

Figure 3a

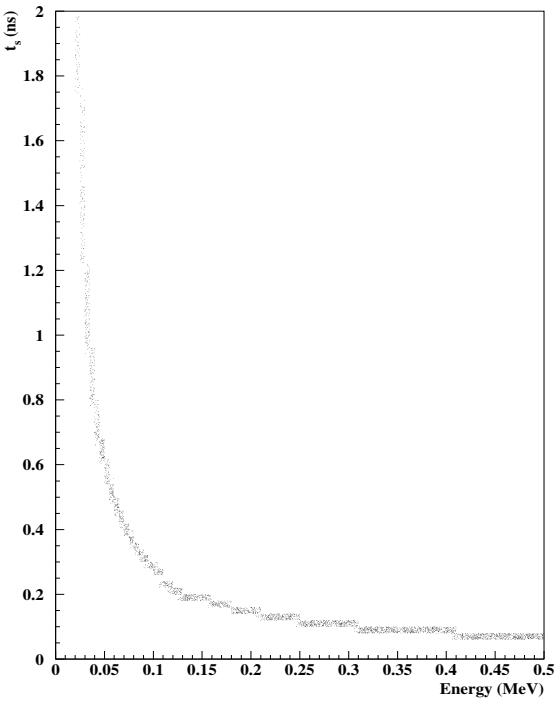

Figure 3b

2.2. The signal rise time.

The shape of the pulse generated at the anode of the PMT is modelled according to the formula:

$$V_a(t) = \frac{q_a}{C} \cdot \frac{\theta}{\tau - \theta} \cdot [exp(-t/\tau) - exp(t/\theta)], \tag{23}$$

where q_a is the charge of the avalanche (the PMT gain is adjusted such that $E = 2$ keV is equivalent to $q_a = 0.25$ pC), θ is the electronic time constant, $C = \theta/R$, where R is the resistance of the integrating circuit.

If the amplitude of the signal calculated in this way is below the lower threshold of the discriminator (V_{th}) the scintillator hit is ignored. On the contrary for a larger signal the hit is considered as detected and the time when the signal reaches the threshold (t_s) is calculated ($V_a(t_s) = V_{th}$). Fig. 3b illustrates the variation of t_s as a function of the energy deposited.

The time when the signal is detected is thus given by:

$$t_{signal} = tof + t_s + tt, \tag{24}$$

where tof is the time of flight of the particle in the detector before reaching the scintillator block, tt is the transit time generated randomly on a Gaussian curve with variance given by relation (22). Time t_{signal} shifted by a constant delay (introduced by the trigger logic) is then coded into a TDC channel number (0.10 ns/channel).

5.2 Geiger cell digitisations

During the process of tracking of a charged particle through the Geiger cells, ionization electrons are generated randomly along the trajectory in the helium gas at a mean rate of one electron per 50 eV energy loss. Delta rays are considered as particles producing themselves ionization electrons. Inside each cell the ionization electron produced closest to the anode wire is considered as responsible for the firing of the wire and its coordinates are stored. In the case of a multiple hit (more than one charged particle crossing the same cell) the electron located nearest to the anode is supposed to fire it.

1. Anode time information.

1.1. Electron diffusion.

While the electron drifts towards the anode wire it suffers longitudinal diffusion with variance:

$$\sigma^2 = \sigma_l \cdot d, \tag{25}$$

where d is the drift distance and σ_l – the longitudinal diffusion coefficient for He.

At T = 300 K and $E/P = 1.6$ V $\cdot$ cm^{-1} $\cdot$ torr^{-1} , $\sigma_l = 0.0026$ cm [25] (E/P is the electric field over pressure ratio).

1.2. Electron drift velocity.

The electron velocity during the drift towards the anode is a complex function of E and of the mean time between elementary collisions (which itself depends on E). In a Geiger cell the electric field varies as a function of the distance to the anode wire, therefore the mean drift velocity for a drift distance d has been approximated by the relation (R_0 is the radius of the wire):

$$w = k \cdot \frac{(R_0 + d) + R_0}{R_0^2 (R_0 + d)^2}. \tag{26}$$

It is known from the literature [25] and from the NEMO prototype [26] that $w = 1$ cm/μs for $d = 1.5$ cm. This allows the value of the constant k to be estimated ($k = 3.74 \cdot 10^{-8}$ cm^4/s).

The drift time t_d is evaluated from the drift distance modified by the drift fluctuations due to the diffusion and from the mean drift velocity. Fig. 4a presents the distribution of t_d as a function of the drift distance for simulated events. This distribution is close to the one obtained from the NEMO 2 experiment [26].

The time when the signal is detected $t_{signal} = tof + t_d$ is shifted by a constant delay (4 μs) and coded into a TDC channel number (20 ns/channel). If the signal occurs after the delay, the time signal is coded by means of a slow TDC at 500 ns/channel (this information allows the detection of delayed α particles).

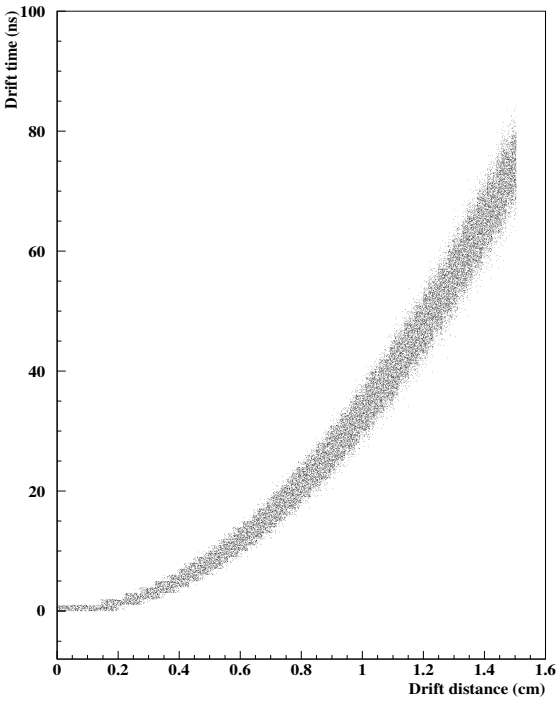

Figure 4a

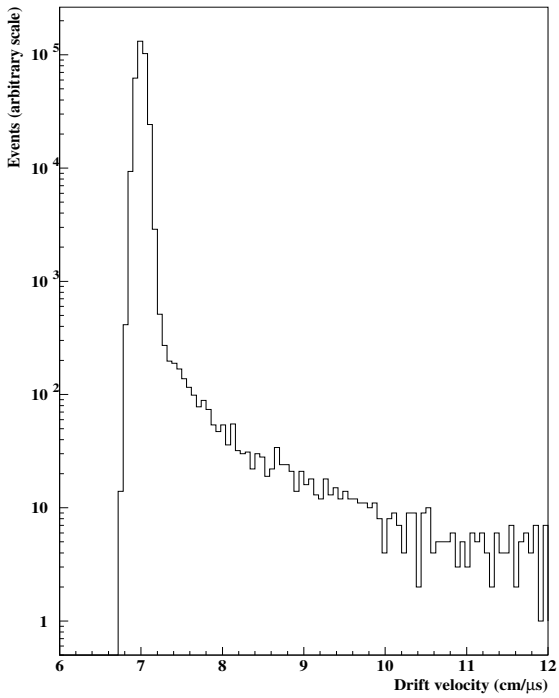

Figure 4b

2. Cathode time information.

The plasma created by the avalanche on the anode propagates towards the extremities of the wire at constant velocity W ($W = 7$ cm/μs) inducing signals on the cathode rings located there. The fluctuation of the drift velocity is supposed to be of the order of 1% as measured in the NEMO 2 prototype and is taken into account. The time signals of both cathodes (t_{kb} and t_{kt}) are coded into TDC channels with a time bin of 20 ns/channel. In the situation where two particles cross the same Geiger cell, two avalanches are supposed to be produced on the same wire and the smallest drift distances on both sides of the wire are used to calculate the plasma drift times. This effect produces a small asymmetry (illustrated in fig. 4b) in the $W = L/(t_{kb} + t_{kt})$ distribution (here L is the anode length) which agrees with the observations made in NEMO 2.

6 Visualization of events

The event visualization part of the program, based on the GEANT drawing package [2], allows the NEMO 3 components, particle trajectories, hits recorded in the sensitive elements of the set up, detectors digitisations and fitted tracks to be visualized. It is especially useful and convenient when used in interactive operation to change the detector representation, understand the behaviour of the events, see the corresponding digitisations and debug pattern recognition programs, but can be also used in batch (to draw some special type of events for example).

Besides the general possibilities of visualization which are provided by the interactive version of GEANT and by PAW, some additional possibilities have been added to offer to

the user useful tools to analyse events (in the future, real data coming from the experiment may be analysed with the same program).

Owing to the creation of view banks containing some drawings of the detector the visualization of hits, tracks etc. is particularly fast (quasi instantaneous on a computer such as an ALPHA workstation) thus making the operator's work specially pleasant.

The current version of the program allows:

- to draw a top view (view along the Z axis) together with a side view (view along the Y or X axis at will) of the detector. The scintillator blocks fired are represented with thick red lines and the energy deposit is indicated. In the top view the Geiger cells hit are represented as circles centered on the corresponding anode wires and of radius proportional to the drift time registered by the TDC's. In the side views a hit is represented by a segment whose length is equal to two times the estimated error on the Z coordinate;
- to zoom any parts of the figures described above. Each zoom operation is always relative to the status of the current zoom parameters which are: the zoom factor and the coordinates of the center of the region to be zoomed simply given to the program by a click by mouse on the screen;
- to superimpose on the drawing the real trajectories taken by the particles. These are represented by the hits recorded during the tracking of the particles (see section 4). It is possible to change the trajectory representation by a continuous line (sometimes needed for more clarity);
- to list the information from the kinematics generated for the event;
- to list the information from the digitisations generated for the event (information described in the banks (see appendix B) and translated into physical quantities);
- to associate digitisations into tracks by clicking on Geiger cell hits present on the screen (a special click ends the accumulation of digitisations). A helix fit is performed through the points collected and the fitted line drawn on the picture;
- to determine the charge of a particle from the curvature of its fitted track (the starting point of the track must be given);
- to modify the association of hits defining a track by adding or removing digitisations. After modification, the track fit is automatically redone with the new associated hits);
- to kill a track;
- to draw the digitisations associated into tracks;
- to list all information relative to the tracks created.

Fig. 5 presents typical zoomed pictures of a simulated $2\beta0\nu$ decay from ^{100}Mo. The relatively low energies of the particles involved lead frequently to events where the trajectories are more complicated. Fig. 6 shows an example of a moderately complex topology obtained from a $2\beta0\nu$ decay from ^{100}Mo.

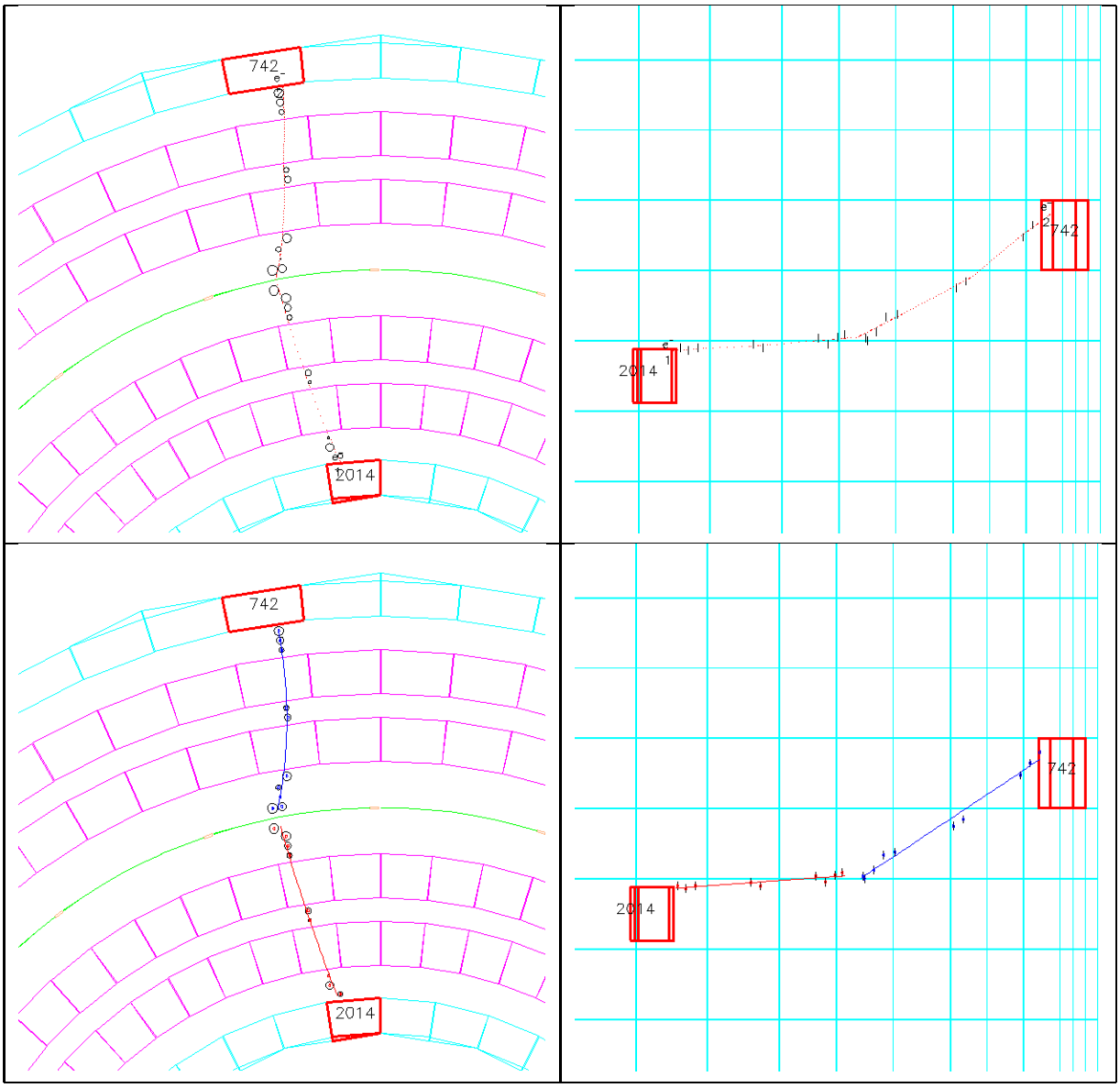

Figure 5: Zoomed pictures of a simulated $2\beta0\nu$ decay from ^{100}Mo: two electrons emerging in opposite directions from the source foil (represented in green) are visible. The pictures on the left (right) are projections on a horizontal (vertical) plane.

The real trajectories followed by the electrons are represented on the top pictures together with the simulated digitisations. The scintillators hit are drawn using thick red lines and the energy deposited (in keV) in each of them is indicated. The Geiger cells hit are represented as circles with radii equal to the drift distance of ionization electrons to the anode wire in the horizontal projection and as segments in the vertical projection.

On the bottom pictures, trajectories obtained by an helix fit through the Geiger cell digitisations are represented. The relatively poor fit of track e_2^- is due to a small angle scatter of the electron e_2 perceptible on the top pictures.

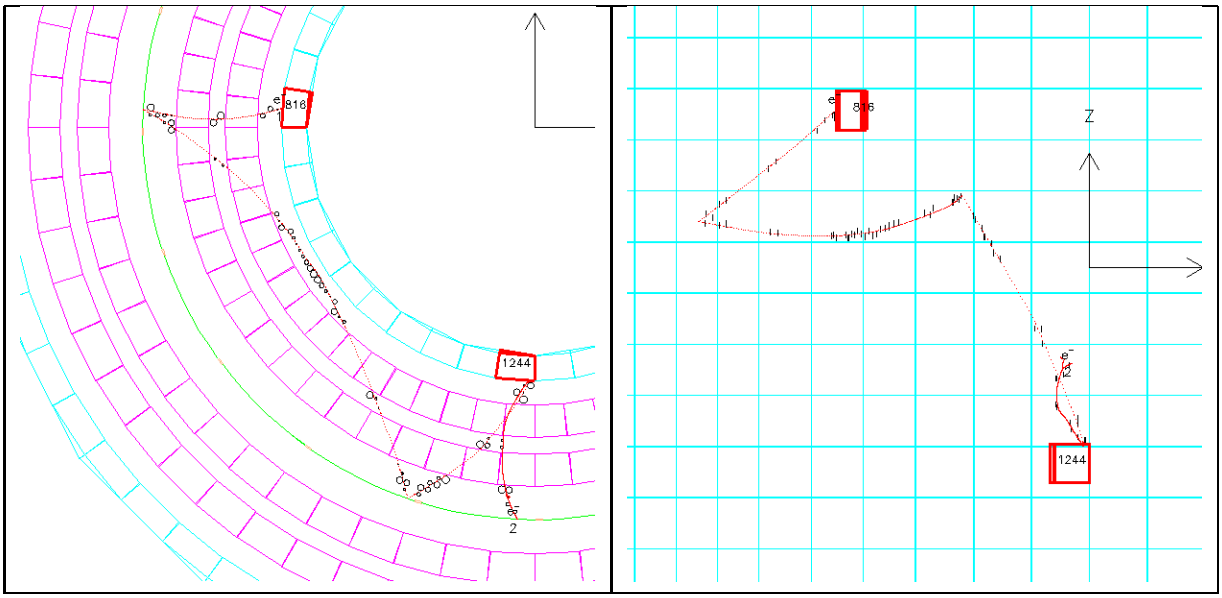

Figure 6: Example of a complex event initiated by a $2\beta0\nu$ decay from ^{100}Mo. The decay point in the foil is visible on the bottom part of the top view (the vertical magnetic field oriented upwards turns the negative particles anticlockwise). Electron e_1 scatters back from the Mo foil and then stops in a scintillator block of the inner wall (top left of the view). Electron e_2 hits a scintillator of the inner wall where it deposits an energy of about 1.2 MeV and scatters back before stopping in the foil (bottom right of the view).

Appendix A

Presently used parameters influencing the tracking step size

The results of the simulation depend critically on the choice of the tracking medium parameters [2]. These parameters influencing the tracking step size are listed below for all tracking media used in the NEMO 3 model. Beside these, the maximum turning angle due to the magnetic field permitted in one step was limited to 5^o.

The parameters DEEMAX, EPSIL and STMIN given below are defined as follows:
DEEMAX – maximum fractional energy loss in one step;
EPSIL – boundary crossing precision (cm);
STMIN – minimum value for the maximum step imposed by energy loss, multiple scattering and magnetic field effects (cm).
A value marked by "*" is calculated by GEANT itself.

Tracking medium	DEEMAX	EPSIL	STMIN
Air	*	0.00010	*
Iron	*	0.00010	*
Copper	*	0.00100	*
Helium	*	0.00010	*
Lightguide	*	0.00010	*
Pmtglass	*	0.00010	*
Magshield	*	0.00100	*
Scintillator	*	0.00010	*
Anode wire	0.05000	0.00010	0.00001
Field wire	0.05000	0.00010	0.00001
Window	*	0.00010	*
Copper tube	*	0.00010	*
Iron shielding	*	0.00010	*
Lead shielding	*	0.00010	*
Mylar wrapping	0.00500	0.00001	0.00001
Teflon wrapping	0.00500	0.00001	0.00001
Polycarbonate	0.22000	0.00200	0.02000
^{100}Mo foils	0.00500	0.00001	0.00001
^{48}Ca foils	0.00500	0.00001	0.00001
^{76}Ge foils	0.00500	0.00001	0.00001
^{82}Se foils	0.00500	0.00001	0.00001
^{96}Zr foils	0.00500	0.00001	0.00001
^{116}Cd foils	0.00500	0.00001	0.00001
^{130}Te foils	0.00500	0.00001	0.00001
^{150}Nd foils	0.00500	0.00001	0.00001

Appendix B

Contents of the **HIT** banks

Detector sets "FOIL" and "WIRE" are not used for the creation of digitisations but for special studies such as intersections of particle tracks with the source foils or diffusions of particles on wires etc...

Scintillators (detector set 'CALO')

1	X	X coordinate of the track (M.R.S.) at the entry into the volume or at creation point (cm)
2	Y	Y coordinate of the track (M.R.S.) at the entry into the volume or at creation point (cm)
3	Z	Z coordinate of the track (M.R.S.) at the entry into the volume or at creation point (cm)
4	FLAG	Flag used during digitisation (1: normal hit, 0: hit has been combined with another hit to form 1 digitisation)
5	U	X of the center of the entrance side of the volume (M.R.S.) (side facing the center of the detector)
6	V	Y of the center of the entrance side of the volume (M.R.S.) (side facing the center of the detector)
7	W	Z of the center of the entrance side of the volume (M.R.S.) (side facing the center of the detector)
8	TOF	T.O.F. of the particle at the entry into the volume or at creation point (ns)
9	E	Kinetic energy of the particle at the entry into the volume or at creation point (GeV)
10	ELOS	Energy loss of the particle inside the volume (GeV)

Geiger cells (detector set 'TKCH')

1	XELE	X coordinate of the ionization electron nearest to the anode wire (M.R.S.) (cm)
2	YELE	Y coordinate of the ionization electron nearest to the anode wire (M.R.S.) (cm)
3	ZELE	Z coordinate of the ionization electron nearest to the anode wire (M.R.S.) (cm)
4	FLAG	Flag used during digitisation (1: normal hit, 0: hit has been combined with another hit to form 1 digitisation)
5	XWIR	X coordinate of the anode wire hit (M.R.S.) (cm)
6	YWIR	Y coordinate of the anode wire hit (M.R.S.) (cm)
7	DMIN	Distance of the nearest ionization electron to the wire (cm)
8	TOF	T.O.F. of the particle at (XELE, YELE, ZELE) (ns)
9	E	Kinetic energy of the particle at the entry into the volume or at creation point (GeV)
10	ELOS	Energy loss of the particle inside the volume (GeV)

Foil (detector set 'FOIL')

1	PX/P	At starting or entrance point in the foil (INWVOL=1) or where the track is leaving (INWVOL=2) or stopping (INWVOL=0)
2	PY/P	At starting or entrance point in the foil (INWVOL=1) or where the track is leaving (INWVOL=2) or stopping (INWVOL=0)
3	PZ/P	At starting or entrance point in the foil (INWVOL=1) or where the track is leaving (INWVOL=2) or stopping (INWVOL=0)
4	FLAG	1000*ISTAK + 100*EFLAG + 10*INWVOL + ISTOP with EFLAG=1 if the charge of the track is -1, else EFLAG=0
5	X	X of the point where the track is leaving the foil (INWVOL=2) or stopping (INWVOL=0) (cm)
6	Y	Y of the point where the track is leaving the foil (INWVOL=2) or stopping (INWVOL=0) (cm)
7	Z	Z of the point where the track is leaving the foil (INWVOL=2) or stopping (INWVOL=0) (cm)
8	TOF0	T.O.F. of the particle at the point where it enters the foil or at creation point (ns)
9	EXYZ	Kinetic energy at point (X, Y, Z) (GeV)
10	ELOS	Energy loss in the foil (GeV)

Wires (detector set 'WIRE')

1	PX/P	At entrance point into the wire (0 if the track is created in the wire)
2	PY/P	At entrance point into the wire (0 if the track is created in the wire)
3	PZ/P	At entrance point into the wire (0 if the track is created in the wire)
4	FLAG	1000*ISTAK+100*EFLAG+10*INWVOL+ISTOP with EFLAG=1 if the charge of the track is -1, else EFLAG=0
5	PX/P	At the point where the track is leaving the wire (INWVOL=2) or stopping (INWVOL=0)
6	PY/P	At the point where the track is leaving the wire (INWVOL=2) or stopping (INWVOL=0)
7	PZ/P	At the point where the track is leaving the wire (INWVOL=2) or stopping (INWVOL=0)
8	TOF0	T.O.F. of the particle at the point where it enters the wire or at creation point (ns)
9	EXYZ	Kinetic energy at point (X, Y, Z) (GeV)
10	ELOS	Energy loss in the wire (GeV)

M.R.S. – Master Reference System

ISTAK – stack track number

INWVOL – 0: track is inside a volume; 1: track has entered a new volume or it is a new track; 2: track is exiting current volume; 3: track is exiting the setup

ISTOP – 0: particle will continue to be tracked; 1: particle has disappeared (decay, inelastic interaction etc.); 2: particle has fallen below the cutoff energy or has interacted but no secondaries have been generated

Contents of the **DIGITISATION** banks

Scintillators — number of bits for coding:

1	DETI	Detector identifier (=0)	[1]
2	SECT	Location: sector number (from 0 to 19)	[5]
3	IOBT	0=inner wall, 1=outer wall, 2=bottom, 3=top	[2]
4	FCLL	For iobt=0 or 1 : 0=first column, 1=central column (outer wall only), 2=last column For iobt=2 or 3 : 0=first crown, 1=second crown, 2=third crown, 3=fourth crown (starting from the center of the detector)	[2]
5	BLOC	Block number (from bottom to top or anticlockwise)	[5]
6	ADC	ADC content for the BLOC	[12]
7	TDC	TDC content for the BLOC	[12]
8	FLAG	Set to 1 if the signal is above the high threshold (0 otherwise)	[1]

Geiger cells

1	DETI	Detector identifier (=1)	[1]
2	SECT	Location: sector number (from 0 to 19)	[5]
3	IO	0=cell located on the inner side of the source foil, 1=cell located on the outer side of the source foil	[1]
4	ABCD	Cell layer: 0 for layer A, 1 for layer B, ..., 8 for layer I (starting from the foil)	[4]
5	CELL	Cell number (from 0 to N counted anticlockwise)	[5]
6	TDCF	Fast TDC content for the cell	[12]
7	TDCS	Slow TDC content for the cell	[12]
8	TDC1	TDC content for cathode 1 (bottom)	[12]
9	TDC2	TDC content for cathode 2 (top)	[12]

References

[1] D. Dassie, R. Eschbarch, F. Hubert et al., "NEMO 3 Proposal. A Proposal for an experiment to study double-beta decay in the search for massive Majorana neutrinos to 0.1 eV", preprint LAL 94-29, Orsay, 1994

[2] "GEANT - Detector description and simulation tool", CERN Program Library Long Writeup W5013, CERN, October 1994

[3] "EUCLID 3", version 1.1F, Matra Datavision, 1994

[4] M. Maire and V. Boninchi, "EUCLID–GEANT interface", version 2-10, IN2P3, 1994

[5] V.I. Tretyak and Yu.G. Zdesenko, "Tables of double beta decay data", At. Data and Nuclear Data Tables 61(1995)43

[6] V.I. Tretyak, "Current possibilities of events generation in GENBB code", NEMO note 6/93, Orsay, 1993

[7] F. Boehm and P. Vogel, "Physics of Massive Neutrinos", 2-nd ed., Cambridge University Press, Cambridge, 1992

[8] M. Doi and T. Kotani, "Neutrino emitting modes of double beta decay", Prog. Th. Phys. 87(1992)1207

[9] M. Doi and T. Kotani, "Neutrinoless modes of double beta decay", Prog. Th. Phys. 89(1993)139

[10] G. Audi and A.H. Wapstra, "The 1995 update to the atomic mass evaluation", Nucl. Phys. A 595(1995)409

[11] V.I. Tretyak, "Monte Carlo algorithms in simulation of 2β decay and penetration of electrons through matter", preprint KINR-92-8, Kiev, 1992

[12] M. Doi, T. Kotani, H. Nishiura, K. Okuda, and E. Takasugi, "Neutrino mass, the right-handed interaction and the double beta decay", Progr. Theor. Phys. 66(1981)1739

[13] R.N. Mohapatra and E. Takasugi, "Neutrinoless double beta decay with double Majoron emission", Phys. Lett. B 211(1988)192

[14] C.P. Burgess and J.M. Cline, "Majorons without Majorana masses and neutrinoless double beta decay", Phys. Lett. B 298(1993)141

[15] C.D. Carone, "Double beta decay with vector majorons", Phys. Lett. B 308(1993)85; private communication (1993)

[16] J.M. Blatt and V.F. Weisskopf, "Theoretical Nuclear Physics", 7-th ed., John Wiley, New York, 1963

[17] G.B. Gelmini and M. Roncadelli, "Left-handed neutrino mass scale and spontaneously broken lepton number", Phys. Lett. B 99(1981)411

[18] V.I. Tretyak, "Models of decay of natural radioactive nuclides", NEMO note 2/92, Orsay, 1992

[19] "Table of isotopes", ed. by C.M. Lederer and V.S. Shirley, 7-th ed., John Wiley, New York, 1978

[20] R.B. Firestone, "Table of isotopes", ed. by V.S. Shirley, 8-th ed., John Wiley, New York, 1996

[21] M. Deutsch and O. Kofoed-Hansen, "Gamma-Rays", in "Experimental nuclear physics", ed. by E. Segre, vol.3, John Wiley, New York, 1959

[22] R.D. Evans, "The Atomic Nucleus", McGraw-Hill Book Comp., New York, 1955

[23] E. Browne and R.B. Firestone, "Table of radioactive isotopes", ed. by V.S. Shirley, John Wiley, New York, 1986

[24] R. Arnold and V.I. Tretyak, "Inox versus field wires in NEMO 3: A Monte Carlo study", note NEMO 9/95, Strasbourg, 1995

[25] A. Peisert and F. Sauli, "Drift and diffusion of electrons in gases: A compilation", preprint CERN 84-08, Geneva, 1984

[26] R. Arnold, A.S. Barabash, Ph. Bernaudin et al., "NEMO 2 detector. Technical report", NEMO note 9/92, Orsay, 1992